UC San Diego

UC San Diego Previously Published Works

Title

The SAMPL5 host—guest challenge: computing binding free energies and enthalpies from explicit solvent simulations by the attach-pull-release (APR) method

Permalink

https://escholarship.org/uc/item/6wc007dx

Journal

Journal of Computer-Aided Molecular Design, 31(1)

ISSN

0920-654X

Authors

Yin, Jian
Henriksen, Niel M
Slochower, David R
et al.

Publication Date

2017

DOI

10.1007/s10822-016-9970-8

Peer reviewed

The SAMPL5 Host-Guest Challenge:

Computing Binding Free Energies and Enthalpies from Explicit Solvent Simulations by the Attach-Pull-Release (APR) Method

Jian Yin, **Niel M. Henriksen**, **David R. Slochower**, and **Michael K. Gilson**[*]

Skaggs School of Pharmacy and Pharmaceutical Sciences, University of California San Diego, La Jolla, California 92093-0736, United States

Abstract

The absolute binding free energies and binding enthalpies of twelve host-guest systems in the SAMPL5 blind challenge were computed using our attach-pull-release (APR) approach. This method has previously shown good correlations between experimental and calculated binding data in retrospective studies of cucurbit[7]uril (CB7) and β-cyclodextrin (βCD) systems. In the present work, the computed binding free energies for host octa acid (OA or OAH) and tetra-endo-methyl octa-acid (TEMOA or OAMe) with guests are in good agreement with prospective experimental data, with a coefficient of determination (R^2) of 0.8 and root-mean-squared error (RMSE) of 1.7 kcal/mol using the TIP3P water model. The binding enthalpy calculations achieve moderate correlations, with R^2 of 0.5 and RMSE of 2.5 kcal/mol, for TIP3P water. Calculations using the newly developed OPC water model also show good performance. Furthermore, the present calculations semi-quantitatively capture the experimental trend of enthalpy-entropy compensation observed, and successfully predict guests with the strongest and weakest binding affinity. The most populated binding poses of all twelve systems, based on clustering analysis of 750 ns molecular dynamics (MD) trajectories, were extracted and analyzed. Computational methods using MD simulations and explicit solvent models in a rigorous statistical thermodynamic framework, like APR, can generate reasonable predictions of binding thermodynamics. Especially with continuing improvement in simulation force fields, such methods hold the promise of making substantial contributions to hit identification and lead optimization in the drug discovery process.

Keywords

SAMPL5; Binding free energy; Binding enthalpy; Host–guest; Force field; Water model

Introduction

Computational approaches employing molecular dynamics (MD) simulations and explicit water models have provided encouraging results in calculations of the binding affinities of

[*]Corresponding author: Prof. Michael K. Gilson, mgilson@ucsd.edu, Telephone: 858-822-0622, Fax: 858-822-7726.

protein-ligand systems, an application of central importance to early-stage drug discovery [1–3]. Compared to widely used docking and scoring methods, MD methods capture more physical details and so promise greater accuracy and more physical insight. Given continued growth in available computing power, it seems probable that MD methods will enhance the role of computation in the critical steps of lead identification and optimization. However, even methods based on MD simulations and explicit water use simplifying approximations; in particular, the potential functions they use are pared down for the sake of maximal computational speed. As a consequence, evaluating and advancing MD-based methods still requires careful comparison with experimental data. For protein-ligand calculations, such comparisons can pose substantial computational challenges, because the size and complexity of proteins make the calculations difficult to converge.

A host-guest system comprises a small guest molecule fitting into the cavity of a somewhat larger host molecule, and held there by attractive noncovalent forces. Much as the E. coli bacterium is a simpler research model for more complex living systems, host-guest systems represent simple models for protein-ligand binding, due to their small size — typically only a few hundred atoms — and limited conformational flexibility; some can also function as components for chemical sensing or drug delivery [4–6]. Different types of host-guest systems exhibit a diversity of binding conformations and a wide range of binding affinities, and thus make a rich library for validating binding calculations. More importantly, computationally demanding methods, such as MD simulations with explicit solvent, can be tested efficiently with host-guest systems, thus avoiding the convergence challenges associated with protein-ligand binding calculations.

The Statistical Assessment of the Modeling of Proteins and Ligands (SAMPL) is an ongoing series of community-wide, blind challenges to assess computational methods related to drug design, allowing testing of computational components including algorithms, solvent models and force fields [7–10]. The challenge of computing properties for which the experimental results are so far unpublished avoids procedural biases that can arise in retrospective analyses. The current 5th SAMPL challenge, SAMPL5, contains two prediction categories: the distribution coefficients of small drug-like molecules between water and cyclohexane, and the binding free energies of host-guest systems. In addition, SAMPL5 is the first round to include the prediction of binding enthalpies for host-guest systems. Binding enthalpies have often been regarded as prohibitively difficult to compute at high precision, because they represent the difference between two large energies, which may have high variances due to the contributions of many solvent molecules. However, our previous studies on cucurbit[7]uril (CB7) have demonstrated that with sufficient sampling and careful implementation, high precision can be achieved in binding enthalpy calculations of host-guest systems [11]. Therefore, a complete thermodynamic profile, comprising the binding free energy, the binding enthalpy, and (by subtraction) the binding entropy, can be obtained and compared with experiment.

Here we report the results of our prospective SAMPL5 host-guest predictions for the host octa acid [12], named OAH in SAMPL5, and its methyl group modified analog [13], OAMe. Note that these compounds are respectively termed octa acid (OA) and tetra-endo-methyl octa-acid (TEMOA) in previous experimental studies [14, 15]. The binding free energies of

both of these hosts, with all six guests in the challenge, were computed using our attach-pull-release (APR) approach [16], and their binding enthalpies were computed with the single-box direct method [16]. The APR free energy calculations use a series of independently simulated windows in which restraints are gradually imposed on the bound guest, used to pull it from the binding cavity, and then released. This approach avoids concerns about possible energy dissipation, and hence irreversibility, associated with nonequilibrium pulling techniques, and also allows efficient distribution of the independent simulations across parallel processors. In our previous retrospective studies of CB7 and β-cyclodextrin (βCD) [16], APR protocols have generated good correlations between experimental and computational binding thermodynamics.

SAMPL5 participants using explicit solvent free energy methods were encouraged to include "standard" runs with a prescribed set of force field and simulation parameters, for at least two of the host-guest systems, to help distinguish when discrepancies between results were caused by procedural differences versus force field differences. In principle, all participants using valid procedures should obtain essentially the same results with these standard setups. Our group generated the standard input files and provided them to the SAMPL5 participants, and then used them as the basis of our own predictions. We also simulated the entire OAH and OAMe set with the exact settings and force field parameters provided to the participants, in advance of receiving the experimental results. In addition, although TIP3P was selected to be the explicit solvent model for standard runs, we also tested the performance of the newly developed OPC water model [17], a three-charge, four-site rigid water model which was optimized to capture the electrostatic properties of the water molecule.

Methods

The chemical structures of OAH, OAMe and their shared guest molecules are shown in Figure 1. Host OAH was previously used in the SAMPL4 challenge [9], but with a different set of guest molecules. Its bowl-shape cavity is surrounded by eight water-solubilizing carboxylate groups: four located at the benzoic acid "flaps" of the binding pocket and four at the pendant propionate chains. The cavity mainly consists of a wide binding region close to the entrance and a gradually narrowing region deeper in the cavity. Host OAMe is identical to OAH, except for the addition of four methyl groups to the cavity entrance. This modification narrows the entrance of the binding pocket [14], sterically reduces the flexibility of the host, and results in significant changes in the binding thermodynamics for the present guests, as detailed below.

Generation of standard input files

The experimental studies were carried out at pH values of 11.3 for NMR and 11.5 for ITC measurements, so both OAH and OAMe were treated as fully deprotonated, with a net charge of $-8e$. Figure 1 shows the protonation state of each guest molecule used in both the standard files and our own simulations. These are assigned based on their putative pKas, and were assumed to remain constant during binding. Bonded and Lennard-Jones parameters were obtained from general AMBER force field (GAFF) [18]. Electrostatic potentials were computed using the Hartree-Fock method in conjunction with 6-31G* basis set, using

Gaussian09 [19], and with the "pop=mk, iop (6/33=2, 6/50=1)" keywords, according to the Merz-Singh-Kollman scheme [20, 21]. Partial atomic charges were then fitted to the electrostatic potentials through the RESP procedure, as implemented in the program Antechamber, with formal charges as drawn in Figure 1. The starting structures of OAH and OAMe were built manually with MOE [22] and then energy minimized. The initial structures of the unbound guest molecules were obtained through the conformational search module in MOE. A 1:1 binding ratio has been confirmed experimentally for all guests and thus been adopted in our calculations. The starting bound configurations were obtained by docking the guests into the hosts with MOE. Earlier experimental studies indicated that charged groups of the guests often locate near the entrance of the cavity while the hydrophobic moieties are always inside the binding pocket [11]. The top ranked binding pose matching these experimental observations was then solvated in a cubic box with 2100 TIP3P water, with sodium ions added only for neutralization. Sodium ions were modeled with the TIP3P-specific sodium parameters of Joung and Cheatham [23]. After a short equilibration phase to relax the solvent, the final frame was saved for distribution to all SAMPL5 participants as the AMBER standard input files for OAH and OAMe. Standard input files in the format of GROMACS, Desmond and LAMPPs formats were converted from the AMBER files with custom scripts [24].

Binding calculations

The binding free energy of each host-guest pair was computed from the work required to attach a set of restraints to the guest and potentially the host molecule (W_{attach}), pull the guest out of the binding pocket (W_{pull}), release all attached restraints ($W_{\text{release-conf}}$), and finally set the guest at standard concentration ($W_{\text{release-std}}$) [16]:

$$\Delta G_{\text{bind}}^0 = -\left(W_{\text{attach}} + W_{\text{pull}} + W_{\text{release-conf}} + W_{\text{release-std}}\right) \quad \text{Eq 1}$$

The translational and rotational host restraints do not perturb the internal conformational degrees of freedom of the host, and remain unchanged during the entire APR process. As a consequence, there is no need to compute the work of attaching and detaching them. For the guest, the restraints were gradually turned on during the attach phase and released in the end. The work of releasing guest restraints was computed analytically. The APR framework is demonstrated in Figure 2. Aided by three dummy atoms, six host restraints (one distance, two angle, and three torsional restraints) were used to keep the host positioned and aligned with the z-axis of the simulation box. Three guest restraints, (one distance and two angle restraints) were imposed to orient the guest on the pulling axis. Please refer to our previous study for more details [16]. Note that the internal degrees of freedom of neither the host nor the guest were affected by this system of restraints. However, for two cases, OAMe-G4 and OAH-G5, additional conformational restraints were imposed and then released, as part of the overall APR process, to solve convergence problems in these particular cases. A total of 14 windows were used for the attach phase, and 46 for the pulling phase. During the pulling phase, the umbrella sampling windows were spaced at 0.4 Å intervals. The guest was pulled to a maximum of 18 Å away from its initial position, at which it was considered to be fully unbound. Each sampling window was simulated for a minimum of 2.5 ns, with extension as

needed to either bring the standard error of the mean (SEM) estimate of the forces under a specified threshold or to 50 ns, whichever came first. The thermodynamic integration (TI) approach [25] was employed to calculate the work terms from the mean force in each window. The force during the attach and release phases is found by taking the partial derivative of the restraint energy with respect to the restraint force constant, as previously detailed [16, 26]. For the pulling phase, it is the partial derivative of the restraint energy with respect to the equilibrium target value of the restraint. The force curves were integrated using trapezium integration of an Akima spline function fit to the force values of each window.

Following prior procedures [16], the binding enthalpies were computed as the difference between the mean potential energy of the first window of the attach phase, which is called the bound state, for which no guest restraints are present, and the last window of the pulling state, which is called the pulled-free state, for which the only restraints are those keeping the guest 18 Å from the host; the energies associated with the restraints themselves were not included in the averages.

Simulation details

Preliminary MD simulations of these systems, for up to a few nanoseconds, were carried out to further relax the solute, and the starting structures for APR were extracted from the last frames. Each system was then re-solvated with 2500 water molecules in an orthorhombic box. The thickness of the water layer between any atom in the solute and the edge of the box was set as 10 Å in the X and Y direction. In the Z direction, the closest distance between the guest and the nearest periodic copy of the host was more than 20 Å, even in the last window, to ensure that the interaction between them would be negligible. The box size was approximately $38 \times 38 \times 55$ Å^3 after equilibration. In addition, different sizes of simulation boxes, which contained 2100 to 5000 water molecules, were tested, and no significant changes on binding free energies were observed.

All APR calculations were performed with the AMBER 14 [27] suite of programs. Binding free energies and binding enthalpies at 298 K were computed for two water models: TIP3P [28] and OPC [17]. Sodium counterions were added only as needed to neutralize the total charge of each host-guest system, due to the low salt concentrations in the corresponding experiments (10–50 mM). The TIP3P-specific ion parameters from Joung and Cheatham [23] were used for the TIP3P simulations, which is consistent with the standard input files, and the hydration free energy set of OPC specific parameters were used for simulations with the OPC water model (see section 3.5 and 3.6 in the AMBER 16 manual [29]). The same bonded and nonbonded parameters as in the standard input files were used. The production phase was simulated in an NPT ensemble with the Berendsen barostat [30] and Langevin thermostat [31]. The cutoff distance of Lennard-Jones interactions was set to 9 Å and a long-range correction was applied to approximate the interactions beyond the cutoff distance [32, 33]. Electrostatic interactions were treated with the particle mesh Ewald (PME) algorithm [34, 35]. SHAKE constraints were applied to bonds involving hydrogen [36, 37], and the simulation time step was set to 2 fs. The binding enthalpies were computed by extending the simulation length of the first and last windows of the APR calculations to 750 ns. The

representative conformations for OAH and OAMe with guests shown in Figure 5 were clustered using 7500 frames (every 100 ps) from each 750 ns bound-state enthalpy simulation via the "cluster" command using the cpptraj program in AMBER 14.

Experimental data for validation

Some guests were measured by both NMR and ITC, while others were studied with only one technique [38]. Thus, there is a somewhat heterogeneous set of experimental data. Here, we compare the calculations with the same set of experimental affinities selected for error analysis in the SAMPL5 overview paper [39]. In the SAMPL5 instruction file released to the participants at the beginning stage of the challenge, the salt concentration conditions of OAH/OAMe systems was described as "aqueous 10mM sodium phosphate buffer at pH 11.5, at 298 K, except for OA-G6, for which the buffer was 50mM sodium phosphate at pH 11.5". Therefore, binding affinities measured at the closest salt conditions were adopted for error analysis. We also computed error metrics based on the averages of available data for each guest, and observed very little difference. For instance, the root mean squared error (RMSE) value of our APR-TIP3P predictions changed from 1.6 to 1.7 kcal/mol.

Adopting a selected NMR/ITC set of binding affinities can sometimes lead to a situation in which an entropy term is obtained by subtracting a binding enthalpy value measured via ITC from a binding affinity value measured via NMR. Although the NMR and ITC measurements had good agreement in most cases, this could potentially generate error, and should thus be kept in mind.

Uncertainties in binding thermodynamics terms

To obtain the SEM of the binding free energy, blocking analysis [40] was used to determine the mean and uncertainty of the restrained coordinates for each umbrella sampling window. Briefly, in blocking analysis, one set of simulations is decomposed into blocks of increasing size, up to a maximum of half the simulation length, and the SEM of the quantity of interest is plotted as a function of block size, using the approximation of statistical independence. The reported SEM is estimated as the maximum value obtained in the plateau of the blocking graph [40].

The uncertainty was then propagated into the potential of mean force (PMF) using bootstrapping [16]. The SEM of the binding enthalpy was generated by first using blocking analysis to obtain the uncertainty of the mean potential energies of the bound and the pulled-free states, and then adding those two in quadrature. The uncertainty in $-T\Delta S$ term was determined by adding the errors of ΔG and ΔH in quadrature. The uncertainties in the error metrics were determined through 100,000 bootstrapping replicates, accounting for both the computational and the experimental uncertainties. For each bootstrap cycle, the composition of the data set was selected "with replacement", with the total number of members equaling twelve (i.e., the size of the original data set). This approach will result in some cycles having multiple copies of a certain host-guest pair and no copies of other pairs, and will provide insight into the dependence of the error metrics on the composition of the data set. To propagate the statistical uncertainty, each member of the bootstrap cycle data set was represented as a normal distribution defined by the mean and SEM for that member. A

random value was chosen from that distribution for each bootstrap cycle, which we term resampling.

Conformational restraints for OAH-G5 and OAMe-G4

During our initial simulations of OAH-G5 and OAMe-G4 systems, we were aware that in some positions during the pulling phase, the distance between the host and guest deviated more than usual from the target distance. In those regions, there were wide gaps between adjacent umbrella sampling windows and the pulling coordinate was poorly sampled. In particular, this occurred when the guest was partially pulling out of the entrance of the host. Such sampling problems were observed in the simulation of OAH-G5 using the TIP3P water model and also in the simulations of OAMe-G4 using both TIP3P and OPC model. However, due to the approaching submission deadline at that time, those issues remained in the predictions. After submission, we addressed this issue much as previously done for the host CB7; i.e., by placing several additional distance restraints across the host entrance to enlarge the cavity in advance of the pulling process [16]. These restraints changed the conformational distribution of the host, and the work of both attaching and releasing them is accounted for APR procedure. The new results are referred to as "corrected" in Table 1.

Results

Binding free energies and binding enthalpies

The experimental and computational binding free energies, enthalpies and entropy contributions for binding of all six guests to the OAH and OAMe hosts are listed in Table 1. The computed binding free energies and enthalpies are also plotted against the experimental results in Figure 3. The error statistics at the bottom of the table were computed across both OAH and OAMe systems. As noted in Methods, the results we submitted to SAMPL5 for OAH-G5 with TIP3P and OAMe-G4 with both TIP3P and OPC reflected inadequate sampling; thus, the corrected binding affinities of OAH-G5 and OAMe-G4 recomputed using conformational restraints are shown in bold, as are the corresponding entropy terms. The submitted predictions are provided in parentheses. For the error statistics, the error metrics involving the corrected affinities and those based on the submitted predictions are similarly listed without and with parentheses, respectively. Two sets of values are also listed similarly for the entropy terms.

The corrected computational results correlate well with the experimental binding free energies, for both the TIP3P and OPC water models, as evident by inspection of Figure 3A and from the coefficient of determination (R^2) values of 0.83 and 0.68 for the two respective water models. The linear regression slopes are close to the unity line, at 1.19 for TIP3P and 0.89 for OPC. There is some systematic error in the computed binding free energies, with mean signed errors (MSE) of −1.59 and −2.14 kcal/mol for TIP3P and OPC, respectively. The computed enthalpies do not correlate as well with experiment as the free energies do, as shown in Figure 3B: the R^2 values are 0.51 for TIP3P and 0.50 for OPC. Again, systematic errors are observed, but they are of opposite sign for TIP3P (MSE −1.31 kcal/mol) and OPC (MSE 2.10 kcal/mol).

When the submitted (uncorrected) predictions for OAH-G5 and OAMe-G4 are used instead of the corrected ones, the overall R^2 values of binding free energies prove to be slightly higher than those based on the corrected results, at 0.90 for TIP3P simulations and 0.77 for OPC, and the MSE, MUE and RMSE values are all slightly lower as well. However, the uncertainty makes the differences in those error metrics of corrected and uncorrected predictions statistically insignificant. The linear regression slopes became larger, at 1.45 for both TIP3P and OPC. In addition, although the corrected affinities of OAH-G5 and OAMe-G4 show larger discrepancies with the corresponding experimental affinities compared to the uncorrected values, they are more consistent with the general observation that the binding free energies were overestimated for both water models.

The phenomenon of enthalpy-entropy compensation was observed across these host-guest series, both experimentally and computationally (Figure 4). For the experimental data, the R^2 value for enthalpy versus $-T S$ is 0.78, with a linear regression slope of -1.22. The OAH-G4 binding pair is an outlier, with a disproportionately small entropy penalty for its binding enthalpy, and this leads to a particularly favorable measured binding free energy of -9.37 kcal/mol. The calculations capture these trends semi-quantitatively. For example, calculations with TIP3P yield compensation with R^2 of 0.55 and calculations with OPC yield R^2 of 0.33, and OAH-G4 is identified as an outlier in both cases, much as seen experimentally. Accordingly, its computed binding free energies are particularly favorable, at -12.34 and -11.35 kcal/mol for TIP3P and OPC, respectively, much as seen experimentally.

Binding modes of OAH and OAMe with guests

Figure 5 shows the most populated binding conformations of OAH and OAMe with each of the six guests, obtained via clustering over 750 ns of simulation time in TIP3P water, for the unrestrained end states used for the enthalpy calculations. Compared to the octa acid guests in the SAMPL4 challenge, the guests tested in SAMPL5 are more diverse, with a variety of chemical groups and different charges. All guests contain a charged hydrophilic head group, which always points upward in Figure 5 and is solvated by water according to the observation in previous experimental studies [12]. The head group is then joined by a hydrophobic moiety, which is either an aliphatic chain, such as in Guest G1 and G3; or an aromatic ring, with or without attached functional group.

Experimental studies on octa acid suggested that cyclic carboxylate guests with extended hydrophobic moieties can reach deeper into the cavity and thus bind more tightly. In the meantime, guests that can only fit into the outer binding region of the cavity tend to bind stronger when a larger portion of the binding regions is occupied [12]. Our simulations revealed that, in the current OAH systems, guests G1–G3 with extended hydrophobic moieties leave plenty of void space in the outer binding region (Figure 5A). By contrast, G4 only resides in the outer binding region of host OAH, but its bulky adamantane core and the bromide moiety fully occupy this region. The strong binding affinity of OAH-G4 (Table 1) suggests that moderately increasing the occupancy of guests in the outer binding region seems to be a more effective way to strengthen binding, compared to making a longer hydrophobic moiety.

The methyl groups in OAMe did not cause any essential change to the guest conformations and orientations in the representative binding modes of OAMe systems (Figure 5B), compared with the corresponding OAH systems (Figure 5A). However, the methyl groups all point toward the region between the charged group and the hydrophobic moiety in each guest, which is usually the slimmest part in the entire guest. Since the methyl groups are in such close contact with most of the bound guests, there is a subtle balance between improving the hydrophobic contacts and causing steric clashes, which we describe in more detail later.

A "flipped" OAH conformation enhanced by guest binding

The flexibility of the pendant propionate chains in OAH and OAMe, as well as some distortion of the binding pockets induced by the bound guests (i.e. breathing motions) were observed in our simulations, and are consistent with those reported in previous computational studies [41]. Another intriguing phenomenon observed in our enthalpy calculations is the flipping of the four benzoic acid "flaps" around the OAH cavity entrance toward the guest (Figure 6A and Figure S1). This occurs occasionally in the unbound state of the enthalpy calculations, in which the OAH host is considered to be free. However, when OAH is bound to a positively charged guest, G3 and G5, this "flipped" conformation becomes dramatically more populated. The flip percentage is 10.15% in both OAH-G3 and OAH-G5, compared to 0.28% in the free OAH. No flipped conformations were observed in the OAMe systems, which may be due to the steric interference between the methyl groups and the guests, and also the insufficient space in the cavity wall for the methyl group when the flap is raised, as demonstrated in Figure 6B.

To our knowledge, this conformational change has not been previously reported in experiments. This could indicate that the observation is an artifact, due to errors in the force field, but there are also reasons it might occur without being noted experimentally. For guests with a negatively charge head group, the flip percentage (Table S1) may be too low to be detected. Meanwhile, the positively charged guests for octa acid were not extensively studied in previous experimental studies. Moreover, even in the case of G3, which generates the highest fraction of flipped conformations, the flip percentage is only about 10%, which is probably still challenging to be detected experimentally, and the possible influence to binding affinity may be insignificant Perhaps guests that can form more attractive electrostatic interactions with the carboxylate groups on OAH could be designed to further increase the flipped population and thus enable verification of this computational observation.

A tale of two host-guest pairs: OAH-G4 and OAMe-G4

The experimental data show high-affinity binding between host OAH and G4, whereas the measured binding affinity of OAMe with the same guest is quite low. Our TIP3P simulations successfully ranked OAH-G4 as the strongest binding pair across the OAH and OAMe systems, and OAMe-G4 as the weakest binding pair out of 12 systems (Table 1). In the OPC simulations, G4 was also computed to have the strongest binding guest for OAH, yet the second weakest binding guest for OAMe. Plausible explanations can be inferred from the

simulations for the unexpected difference of binding affinities between the OAH-G4 and OAMe-G4 systems.

First, both calculation and experiment show a large enthalpy contribution to binding of OAH with G4, which can be related to the close and favorable contacts between these compounds in the bound state (Figure 5). This is consistent with our previous observations that the adamantane guests are more enthalpically favorable than other guests due to a better steric fit when they bind to CB7 [11]. Additionally, this particularly favorable enthalpic contribution in OAH-G4 is not associated with a commensurate entropy loss (Figure 4). For the OAMe-G4 system, the measured enthalpy value is not available, but the simulations allow one to speculate about why its affinity is so much less. Given that the binding modes of OAH- and OAMe-G4 are quite similar, we visually inspected the actual MD trajectories for both systems. Interestingly, in the binding pocket of OAH, G4 rotates much more freely than in the cavity of OAMe, with the bromide group pointing in all directions. In contrast, in OAMe, the motions of this guest are greatly restricted by this host's added methyl groups. Based on these observations, we conjecture that, although the methyl groups in OAMe in general provide close favorable contacts with the various guest molecules, they also restrict the motion of the guest, leading to a greater entropic penalty, relative to binding to OAH. In the case of G4, the restriction may become much more severe, due to the bulky adamantane core as well as the large bromine atom, leading to reduced binding affinity.

Meanwhile, it is uncertain whether reduced freedom of the guest in this situation can account for the full entropy drop; other factors, such as changes in water structure, may also contribute.

Comparing standard runs from different research groups

Another SAMPL5 host-guest submission, SOMD-3 from Dr. Julien Michel's group [42], used the standard simulation files generated by our setup procedures (see Methods), and thus should, in principle give results very similar to our TIP3P calculations. The name SOMD indicates MD simulations conducted within the Sire [43] and OpenMM [44] framework. Instead of computing the work along a physical dissociation pathway, as done in APR, SOMD-3 used the double decoupling method [45, 46] with a single topology approach and the multistate Bennett acceptance ratio (MBAR) [47] method. In principle, the present APR-TIP3P results and those from the SOMD-3 submission should agree to within numerical error, and 9 of the 12 SOMD-3 binding free energies in fact match our submitted predictions to within 1 kcal/mol, which is reasonable in light of the numerical precision of the methods. The discrepancy for OAMe-G4 was resolved when we improved the sampling for this case (see above), but the disagreements for OAH-G5 and OAMe-G5 persist, despite our rerunning OAH-G5 with host conformational restraints and the SOMD-3 group running additional replicates. Currently, the computed binding free energies for OAH-G5 are -6.9 ± 0.1 kcal/mol and -4.5 ± 0.5 kcal/mol from SOMD-3 and APR-TIP3P, respectively; and the binding affinities of OAMe-G5 are -6.5 ± 0.3 kcal/mol from SOMD versus -5.3 ± 0.2 kcal/mol from APR-TIP3P. The overall root-mean-squared deviation between SOMD-3 and APR-TIP3P, with matched parameters, is 0.9 kcal/mol across all 12 of the OAH and OAMe systems.

Discussion

The binding free energies computed using our APR approach for the SAMPL5 challenge achieved good correlations with measured values, although the deviations from the absolute experimental binding affinities are still large compared to the oft-stated goal of predicting protein-ligand binding affinities to within ~1 kcal/mol accuracy. The binding enthalpy calculations only revealed moderate correlations, despite good convergence indicated by high numerical precision. The TIP3P water model outperformed OPC model for the SAMPL5 series of systems as a whole, but more assessment based on larger test sets is needed to further evaluate the performance of water models on binding calculations. Additionally, the choice of force field parameters for the hosts and guests might influence this result.

Divergent results were observed in binding enthalpy calculations using the two different water models. The newly developed OPC water tended to underestimate binding enthalpies, whereas the TIP3P water model tended to yield overestimates. One possible explanation is that the OPC water model has a larger dispersion coefficient for the van der Waals interactions, relative to TIP3P, and thus may tend to energetically favor states in which the solutes interact with water rather than each other. Another possible reason is their different behavior in the presence of dissolved salt, as suggested by our prior studies showing that the salt effect on computed binding enthalpies for a cucurbituril-guest system differ sharply between these, as well as other, water models [48]. Further explorations of how water models and dissolved salt affect computed binding thermodynamics calculations are being carried out in our ongoing work.

Enthalpy-entropy compensation was observed for all guests in OAH and OAMe systems, though to a smaller degree in the case of G4. The fact that OAH-G4 can to some degree overcome the seemingly ubiquitous occurrence of enthalpy-entropy compensation and achieve high-affinity binding through a more favorable binding enthalpy points to the possibility of designing binding systems that gain affinity by deviating from the compensation trend. For the OAMe-G4 system, the low binding affinity was mainly attributed to a drastic entropy loss, based on the TIP3P simulations results. Our simulations capture the enthalpy-entropy compensation phenomenon and replicate and correctly highlight the distinctive binding thermodynamics of the of OAH-G4 and OAMe-G4 systems. Furthermore, the simulations allow one to inspect the most populated binding modes, and thus to plausibly interpret the balance of forces that influence the binding process on a physical basis.

The issues of inadequate sampling we encountered in the OAH-G5 and OAMe-G4 systems were revealed by examining the histograms of restrained distances between one of the anchor particles and the guest. Note that complete lack of overlap between successive windows along the PMF does not yield large error bars in the MBAR results, and must instead by identified by inspection. In the past, similar issues were encountered when computing the binding free energies of various CB7 systems using the APR approach, but this did not arise in cyclodextrin calculations [16]. Meanwhile, among the SAMPL5 OAH and OAMe systems, only OAH-G5 and OAMe-G4 appeared to be problematic. Given the

unpredictable occurrence of this problem, and the fact that it may not manifest in the reported numerical uncertainty, examining the distance histogram should become a routine step in the APR protocol for every system.

In summary, our APR approach generated reasonably good, but still imperfect, predictions of binding free energies for the OAH and OAMe systems in the SAMPL5 challenge. The computed binding enthalpies did not correlate with experiment very well, but still provided semi-quantitative agreement with experiment, which allowed drawing at least plausible conclusions regarding determinants of binding affinity. This technology might thus find application in the challenge of lead optimization. Overall, there is still room to improve the accuracy of binding thermodynamics calculations of the host-guest systems. The similar binding free energies produced in our calculations using different water models suggest that the improvement of binding calculations gained through optimizing water parameters could be limited. Instead, accurate parameters of the general force field for the ligands or more advanced energy functions may be more important to generate meaningful improvement in affinity predictions.

Supplementary Material

Refer to Web version on PubMed Central for supplementary material.

Acknowledgments

References

1. Durrant JD, McCammon JA. Molecular dynamics simulations and drug discovery. BMC Biol. 2011; 9:71. 10.1186/1741-7007-9-71. [PubMed: 22035460]

2. Deng Y, Roux B. Computations of standard binding free energies with molecular dynamics simulations. J Phys Chem B. 2009; 113:2234–2246. DOI: 10.1021/jp807701h. [PubMed: 19146384]

3. Wang L, Wu Y, Deng Y, et al. Accurate and reliable prediction of relative ligand binding potency in prospective drug discovery by way of a modern free-energy calculation protocol and force field. J Am Chem Soc. 2015; 137:2695–2703. DOI: 10.1021/ja512751q. [PubMed: 25625324]

4. Yallapu MM, Jaggi M, Chauhan SC. Poly(beta-cyclodextrin)/Curcumin Self-Assembly: A Novel Approach to Improve Curcumin Delivery and its Therapeutic Efficacy in Prostate Cancer Cells. Macromol Biosci. 2010; 10:1141–1151. DOI: 10.1002/mabi.201000084. [PubMed: 20572274]

5. Hamasaki K, Ikeda H, Nakamura A, et al. Fluorescent sensors of molecular recognition. Modified cyclodextrins capable of exhibiting guest-responsive twisted intramolecular charge transfer fluorescence. J Am Chem Soc. 1993; 115:5035–5040. DOI: 10.1021/ja00065a012.

6. Zhang B, Isaacs L. Acyclic cucurbit[n]uril-type molecular containers: Influence of aromatic walls on their function as solubilizing excipients for insoluble drugs. J Med Chem. 2014; 57:9554–9563. DOI: 10.1021/jm501276u. [PubMed: 25369565]

7. Geballe MT, Skillman AG, Nicholls A, et al. The SAMPL2 blind prediction challenge: Introduction and overview. J Comput Aided Mol Des. 2010; 24:259–279. DOI: 10.1007/s10822-010-9350-8. [PubMed: 20455007]

8. Muddana HS, Varnado CD, Bielawski CW, et al. Blind prediction of host-guest binding affinities: a new SAMPL3 challenge. J Comput Aided Mol Des. 2012; 26:475–87. DOI: 10.1007/s10822-012-9554-1. [PubMed: 22366955]

9. Muddana HS, Fenley AT, Mobley DL, Gilson MK. The SAMPL4 host-guest blind prediction challenge: An overview. J Comput Aided Mol Des. 2014; 28:305–317. DOI: 10.1007/s10822-014-9735-1. [PubMed: 24599514]

10. Mobley DL, Wymer KL, Lim NM, Guthrie JP. Blind prediction of solvation free energies from the SAMPL4 challenge. J Comput Aided Mol Des. 2014; 28:135–150. DOI: 10.1007/s10822-014-9718-2. [PubMed: 24615156]

11. Fenley AT, Henriksen NM, Muddana HS, Gilson MK. Bridging Calorimetry and Simulation through Precise Calculations of Cucurbituril – Guest Binding Enthalpies. J Chem Theory Comput. 2014; 10:4069–4078. [PubMed: 25221445]

12. Gibb CLD, Gibb BC. Binding of cyclic carboxylates to octa-acid deep-cavity cavitand. J Comput Aided Mol Des. 2014; 28:319–325. DOI: 10.1007/s10822-013-9690-2. [PubMed: 24218290]

13. Gan H, Benjamin CJ, Gibb BC. Nonmonotonic assembly of a deep-cavity cavitand. J Am Chem Soc. 2011; 133:4770–4773. DOI: 10.1021/ja200633d. [PubMed: 21401093]

14. Gan H, Gibb BC. Guest-mediated switching of the assembly state of a water-soluble deep-cavity cavitand. Chem Commun. 2013; 49:1395–1397. DOI: 10.1039/c2cc38227j.

15. Jordan JH, Gibb BC. Molecular containers assembled through the hydrophobic effect. Chem Soc Rev. 2014; 44:547–585. DOI: 10.1039/c4cs00191e.

16. Henriksen NM, Fenley AT, Gilson MK. Computational Calorimetry: High-Precision Calculation of Host-Guest Binding Thermodynamics. J Chem Theory Comput. 2015; 11:4377–4394. DOI: 10.1021/acs.jctc.5b00405. [PubMed: 26523125]

17. Izadi S, Anandakrishnan R, Onufriev AV. Building Water Models : A Different Approach. J Phys Chem Lett. 2014; 5:3863–3871. [PubMed: 25400877]

18. Wang J, Wolf RM, Caldwell JW, et al. Development and Testing of a General Amber Force Field. 2004; 25:1157–1174.

19. Frisch, MJ.; Trucks, GW.; Schlegel, HB.; Scuseria, GE.; Robb, MA.; Cheeseman, JR.; Scalmani, G.; Barone, V.; Mennucci, B.; Petersson, GA.; Nakatsuji, H.; Caricato, M.; Li, X.; Hratchian, HP.; Izmaylov, AF.; Bloino, J.; Zheng, G.; Sonnenberg, JL.; Had, M.; F, DJ. Revision D.01. Wallingford: Gaussian Inc; 2013. Gaussian 09. DOI: 10.1017/CBO9781107415324.004

20. Singh UC, Kollman Pa. An approach to computing electrostatic charges for molecules. J Comput Chem. 1984; 5:129–145. DOI: 10.1002/jcc.540050204.

21. Besler BH, Merz KM, Kollman Pa. Atomic charges derived from semiempirical methods. J Comput Chem. 1990; 11:431–439. DOI: 10.1002/jcc.540110404.

22. Molecular Operating Environment (MOE) 2013.08. 1010 Sherbooke St. West, Suite #910, Montreal, QC, Canada: Chemical Computing Group Inc.; 2016. H3A 2R7

23. Joung IS, Cheatham TE. Determination of alkali and halide monovalent ion parameters for use in explicitly solvated biomolecular simulations. J Phys Chem B. 2008; 112:9020–9041. DOI: 10.1021/jp8001614. [PubMed: 18593145]

24. Shirts MR, Klein C, Swails JM, et al. Lessons learned from comparing molecular dynamics engines on the SAMPL5 dataset. J Comput Aided Mol Des. 2016 DOI: 10.1007/s10822-016-9977-1.

25. Kirkwood JG. Statistical Mechanics of Fluid Mixtures. J Chem Phys. 1935; 3:300–313. DOI: 10.1063/1.1749657.

26. Velez-Vega C, Gilson MK. Force and stress along simulated dissociation pathways of cucurbituril-guest systems. J Chem Theory Comput. 2012; 8:966–976. DOI: 10.1021/ct2006902. [PubMed: 22754402]

27. Case, DA.; Babin, V.; Berryman, JT., et al. AMBER. Vol. 14. San Francisco: University of California; 2014.

28. Jorgensen WL, Chandrasekhar J, Madura JD, et al. Comparison of simple potential functions for simulating liquid water. J Chem Phys. 1983; 79:926–935. DOI: 10.1063/1.445869.

29. Case, DA.; Betz, RM.; Botello-Smith, W.; Cerutti, DS.; Cheatham, TE., III; Darden, TA.; Duke, RE.; Giese, TJ.; Gohlke, H.; Goetz, AW.; Homeyer, N.; Izadi, S.; Janowski, P.; Kaus, J.;

Kovalenko, A.; Lee, TS.; LeGrand, S.; Li, P.; Lin, C. PA AMBER. Vol. 16. San Francisco: University of California; 2016.

30. Berendsen HJC, Postma JPM, van Gunsteren WF, et al. Molecular dynamics with coupling to an external bath. J Chem Phys. 1984; 81:3684–3690. DOI: 10.1063/1.448118.

31. Loncharich RJ, Brooks BR, Pastor RW. Langevin dynamics of peptides: The frictional dependence of isomerization rates of N-acetylalanyl-N'-methylamide. Biopolymers. 1992; 32:523–535. DOI: 10.1002/bip.360320508. [PubMed: 1515543]

32. Shirts MR, Mobley DL, Chodera JD, Pande VS. Accurate and efficient corrections for missing dispersion interactions in molecular simulations. J Phys Chem B. 2007; 111:13052–13063. DOI: 10.1021/jp0735987. [PubMed: 17949030]

33. Wu X, Brooks BR. Isotropic periodic sum: A method for the calculation of long-range interactions. J Chem Phys. 2005 DOI: 10.1063/1.1836733.

34. Darden T, York D, Pedersen L. Particle mesh Ewald: An N log(N) method for Ewald sums in large systems. J Chem Phys. 1993; 98:10089. DOI: 10.1063/1.464397.

35. Essmann U, Perera L, Berkowitz ML, et al. A smooth particle mesh Ewald method. J Chem Phys. 1995; 103:8577–8593. DOI: 10.1063/1.470117.

36. Ryckaert JP, Ciccotti G, Berendsen HJC. Numerical integration of the cartesian equations of motion of a system with constraints: molecular dynamics of n-alkanes. J Comput Phys. 1977; 23:327–341. DOI: 10.1016/0021-9991(77)90098-5.

37. Miyamoto S, Kollman PA. SETTLE: an analytical version of the SHAKE and RATTLE algorithm for rigid water models. J Comput Chem. 1992; 13:952–962. DOI: 10.1002/jcc.540130805.

38. Sullivan MR, Sokkalingam P, Nguyen T, et al. Binding of carboxylate and trimethylammonium salts to octa-acid and TEMOA deep-cavity cavitands. J Comput Aided Mol Des. 2016 DOI: 10.1007/s10822-016-9925-0. (ahead of print).

39. Yin J, Henriksen NM, Slochower DR, et al. Overview of the SAMPL5 host-guest challenge: are we doing better? J Comput Aided Mol Des. 2016 DOI: 10.1007/s10822-016-9974-4.

40. Flyvbjerg H, Petersen HG. Error estimates on averages of correlated data. J Chem Phys. 1989; 91:461–466. DOI: 10.1063/1.457480.

41. Mikulskis P, Cioloboc D, Andreji M, et al. Free-energy perturbation and quantum mechanical study of SAMPL4 octa-acid host-guest binding energies. J Comput Aided Mol Des. 2014; 28:375–400. DOI: 10.1007/s10822-014-9739-x. [PubMed: 24700414]

42. Bosisio S, Mey ASJS, Michel J. Blinded predictions of host-guest standard free energies of binding in the SAMPL5 challenge. J Comput Aided Mol Des. 2016 DOI: 10.1007/s10822-016-9933-0. (ahead of print).

43. Woods CJW, Mey A, Calabro G, Michel J. Sire Molecular Simulations Framework. 2016 [Accessed July 28th] http://siremol.org.

44. Eastman P, Friedrichs MS, Chodera JD, et al. OpenMM 4: A reusable, extensible, hardware independent library for high performance molecular simulation. J Chem Theory Comput. 2013; 9:461–469. DOI: 10.1021/ct300857j. [PubMed: 23316124]

45. Gilson MK, Given JA, Bush BL, McCammon JA. The statistical-thermodynamic basis for computation of binding affinities: a critical review. Biophys J. 1997; 72:1047–1069. DOI: 10.1016/S0006-3495(97)78756-3. [PubMed: 9138555]

46. Boresch S, Tettinger F, Leitgeb M, Karplus M. Absolute Binding Free Energies: A Quantitative Approach for Their Calculation. J Phys Chem B. 2003; 107:9535–9551.

47. Shirts MR, Chodera JD. Statistically optimal analysis of samples from multiple equilibrium states. J Chem Phys. 2008; 129:124105. DOI: 10.1063/1.2978177. [PubMed: 19045004]

48. Gao K, Yin J, Henriksen NM, et al. Binding Enthalpy Calculations for a Neutral Host–Guest Pair Yield Widely Divergent Salt Effects across Water Models. J. Chem. Theory Comput. 2015; 11:4555–4564. [PubMed: 26574247]
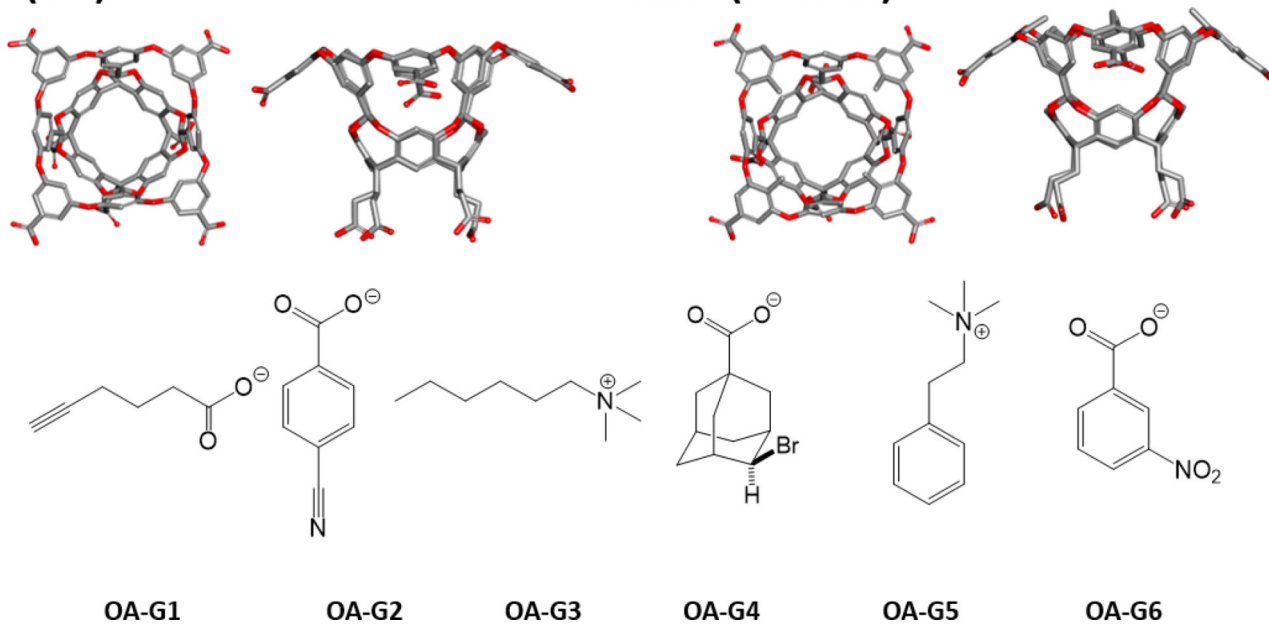
Fig 1.
Chemical structures of hosts OAH and OAMe (also known as OA and TEMOA) in top and side views, along with their shared guests G1–G6.
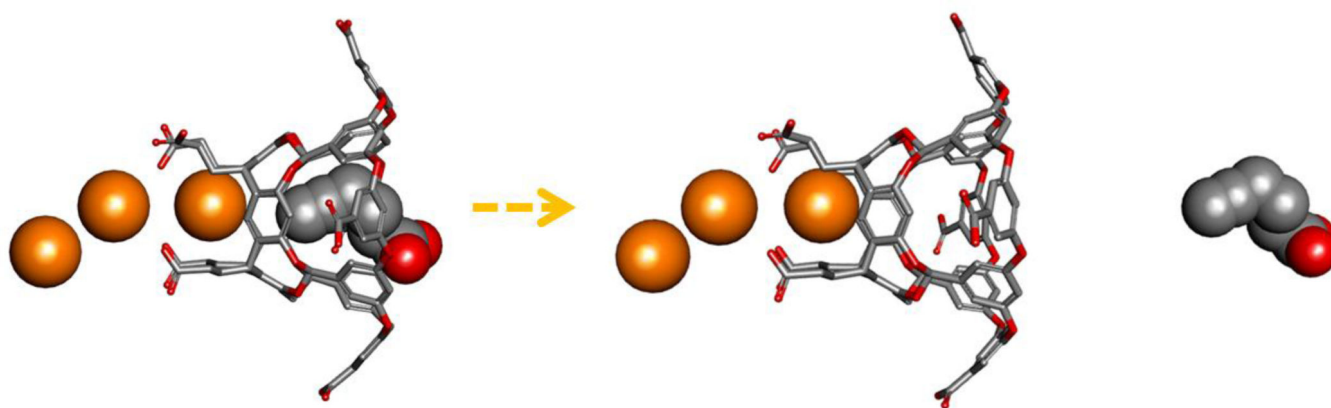
Fig 2.
Diagram of the APR setup. The OAH host is in bond-stick representation, and the guest and anchor particles are in space-filling CPK representation. Silver: carbon; Red: oxygen; Orange: anchor particle. Hydrogen atoms are omitted for clarity. The three anchor particles are dummy atoms used to align the host and the guest with the z-axis of the simulation box. The guest is pulled from the binding site into solution, through a series of closely spaced, independent simulation windows.
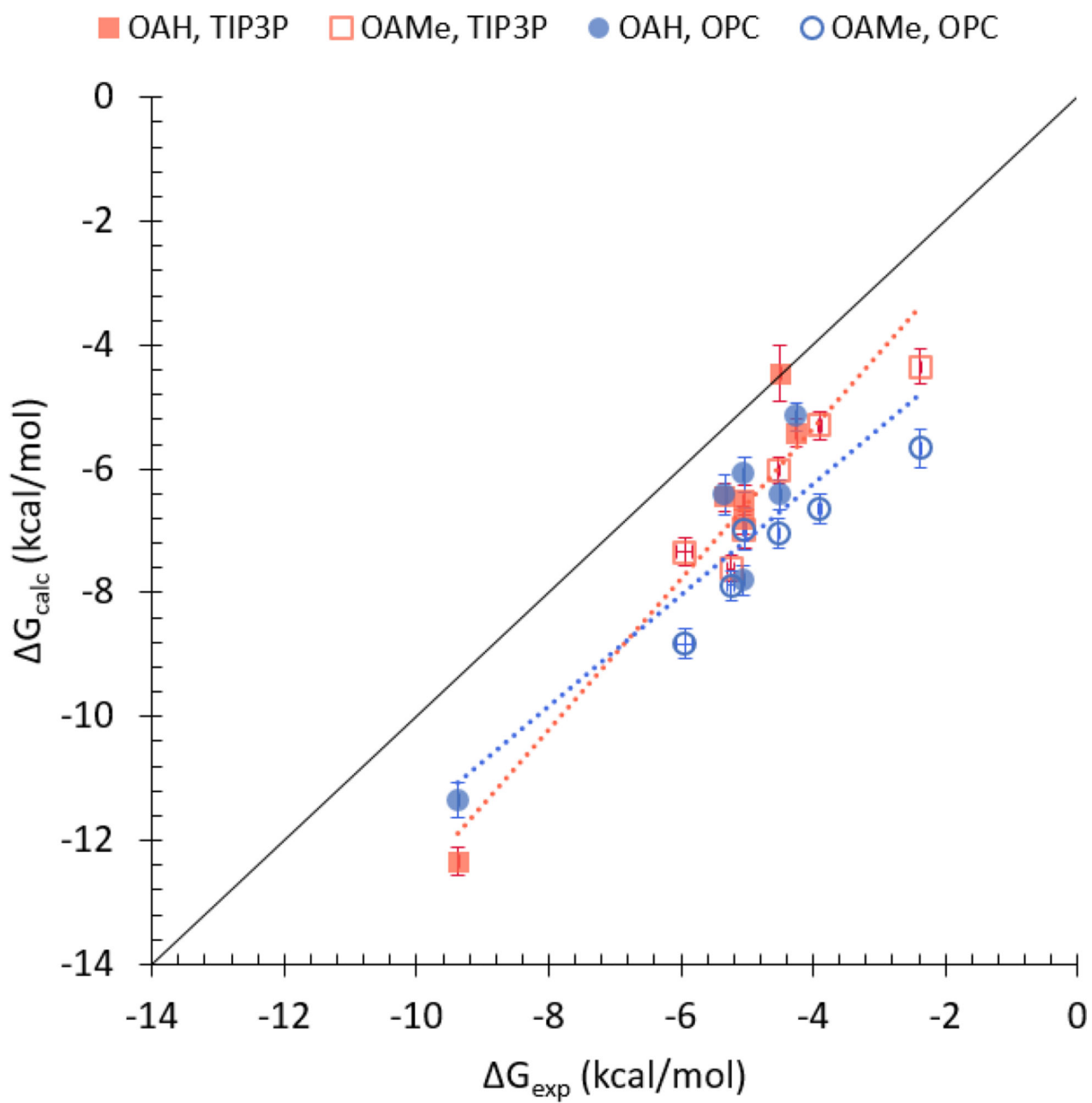
**(A)**
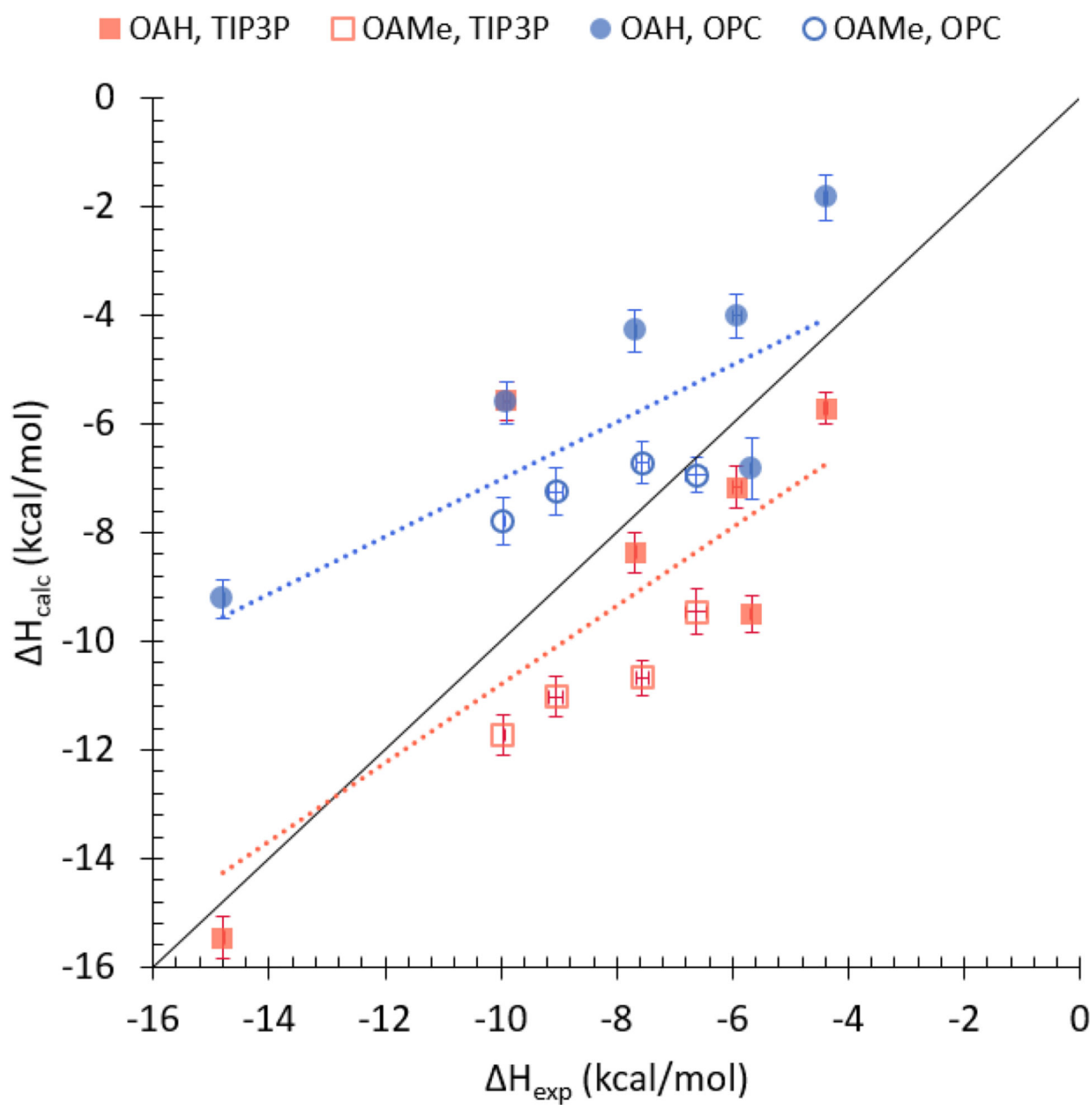
(B)

Fig 3.
Scatter plots of computed versus experimental (A) binding free energies and (B) binding enthalpies for the combined OAH (filled symbols) and OAMe (open symbols) datasets. The corrected binding affinities are plotted for OAH-G5 and OAMe-G4 systems. Red squares: TIP3P results; blue circles: OPC results. Horizontal bars indicate the experimental uncertainties (SEM) although some of them are too small to be visible. Vertical bars indicate the computational uncertainties (SEM). Solid black line is the line of identity.
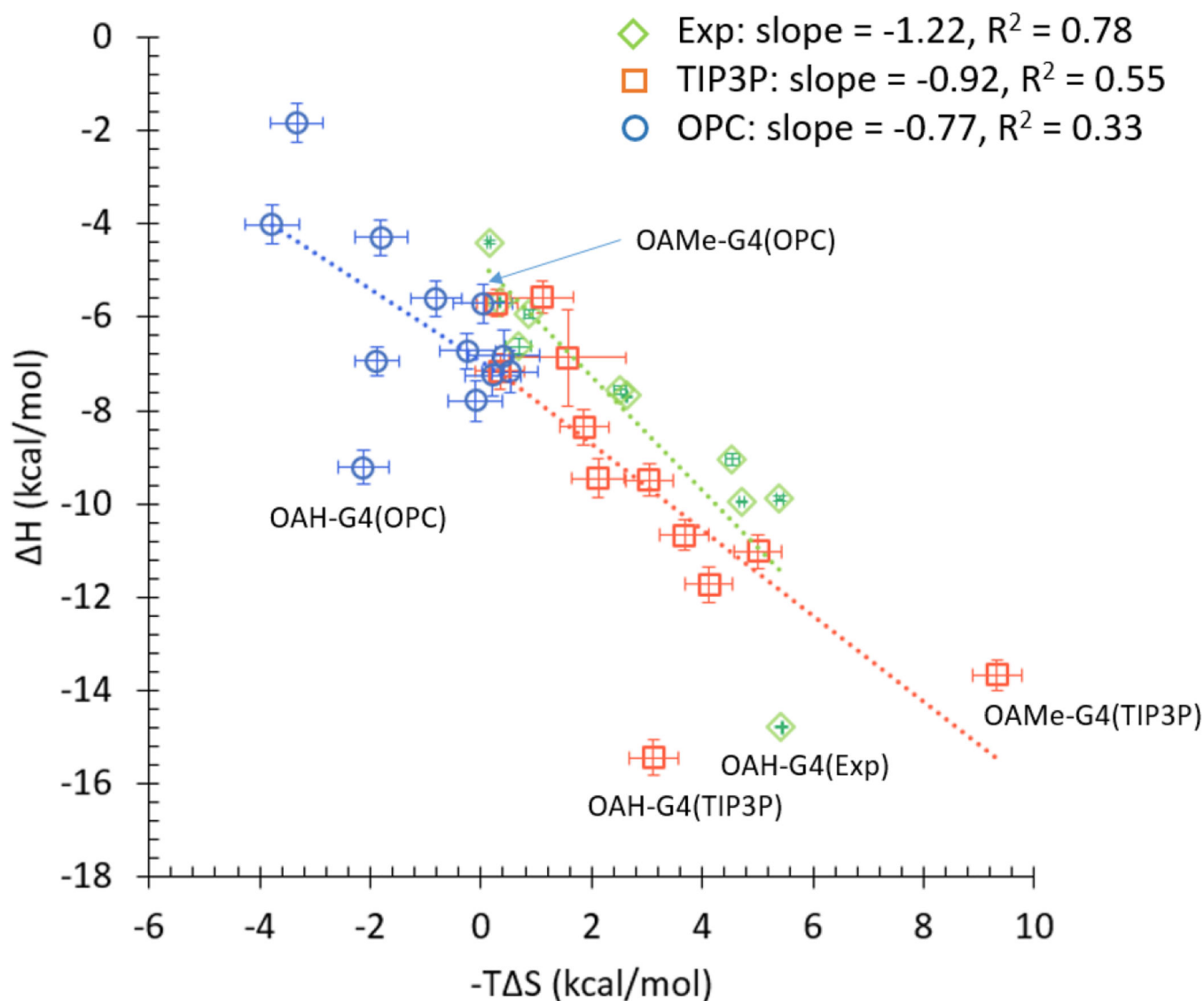
Fig 4.
Scatter plots of binding enthalpy versus the entropic contribution to the free energy, for the combined OAH and OAMe dataset. The corrected binding thermodynamics are plotted for the OAH-G5 system. Green diamonds: experimental values (exp.); red squares: TIP3P data; blue circles: OPC data. Vertical and horizontal bars indicate the uncertainties for ΔH and −TΔS, respectively. Solid black line is the line of identity. Note that experimental binding enthalpies are not available for OAMe-G4 and OAMe-G5.

(A)

(B)
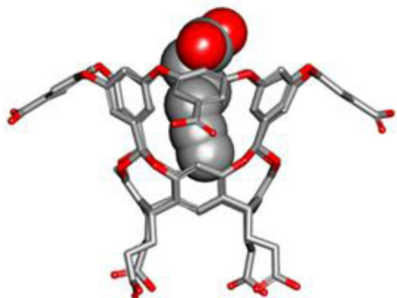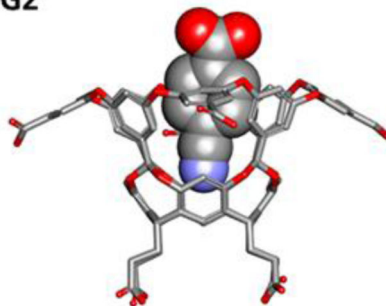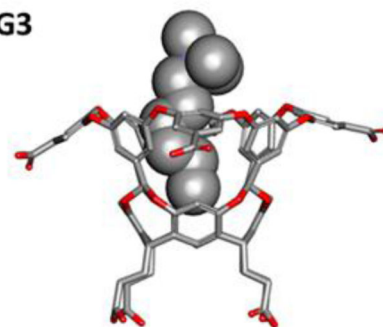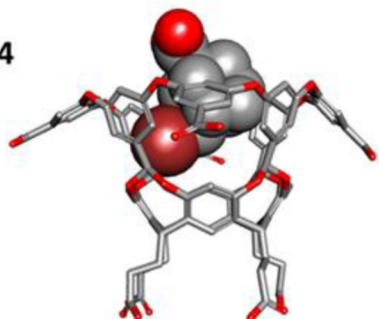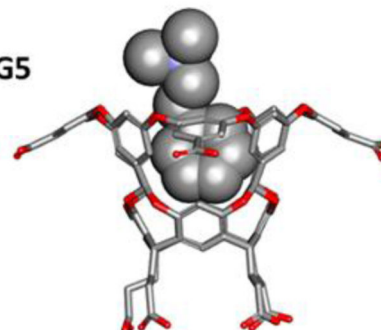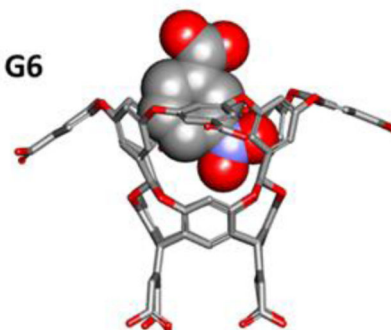
Fig 5.
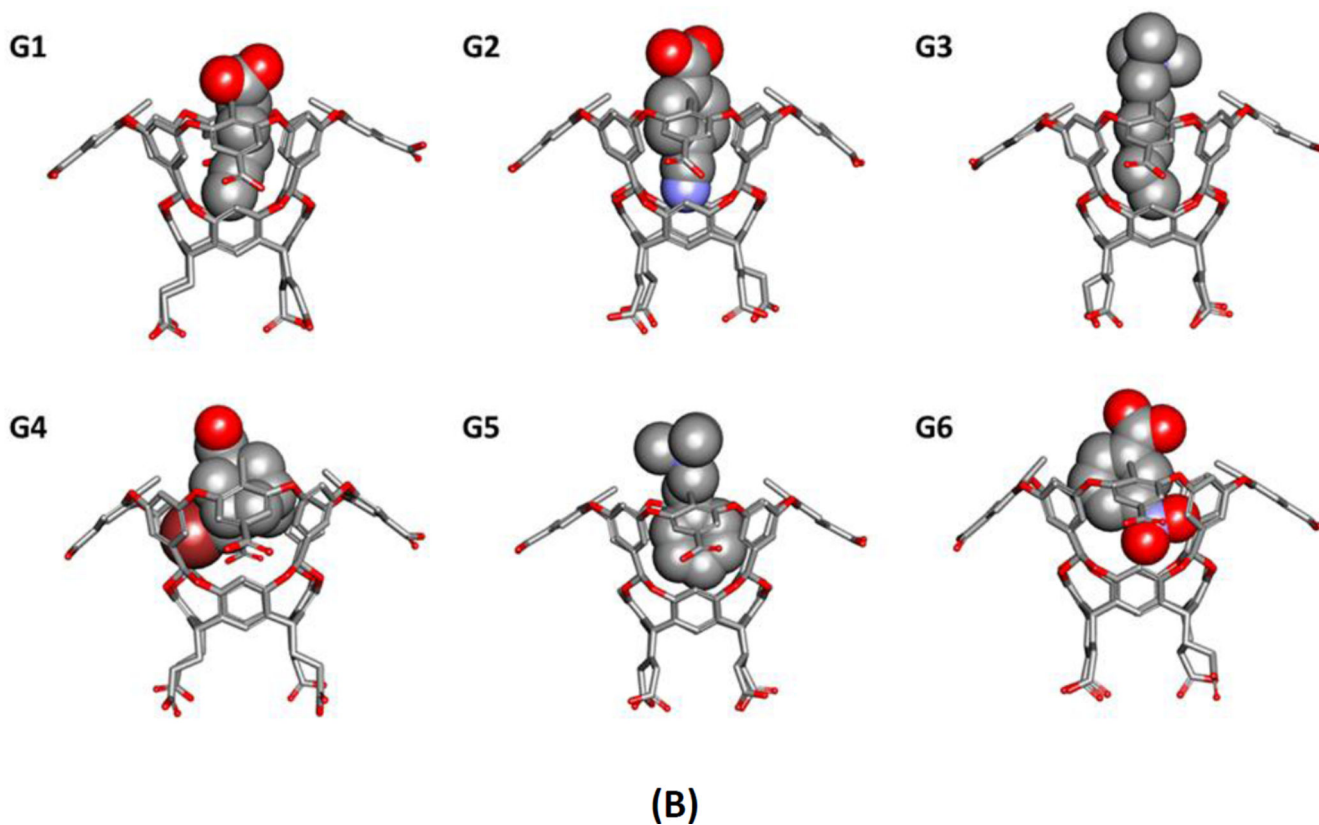The representative binding mode of each guest bound to (A) OAH and (B) OAMe. Silver: carbon; Red: oxygen; Blue: nitrogen; Brown: bromine. Hydrogen atoms were omitted for clarity. All structures were obtained via clustering over 750 ns of MD simulations using TIP3P water model. The host molecules are in a stick-bond representation and the guest molecules are in a space-filling representation.
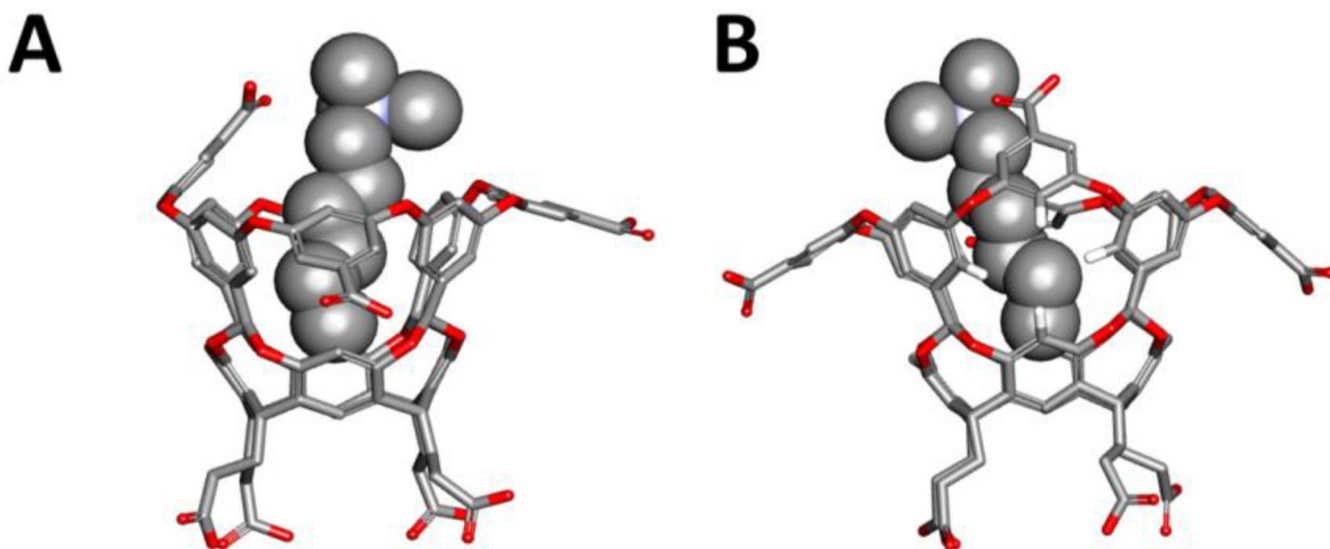
Fig 6.
The "flipped" conformation of OAH-G3, from two viewpoints (A and B). Hydrogen atoms are omitted for clarity, except for those on the cavity wall and near the upward-pointing carboxylate group in b.

Table 1

Experimental and computed binding thermodynamics (kcal/mol) of OAH and OAMe systems. Calculated results are provided for the standard setups provided to participants (TIP3P), and for otherwise matched calculations using the OPC water model in place of TIP3P (OPC). R^2 (correlation of determination) and slope were obtained from linear regression fitting. MSE: mean signed error; MUE: mean unsigned error; RMSE: root mean squared error.

System	G			H			−T S		
	Exp.	TIP3P	OPC	Exp.	TIP3P	OPC	Exp.	TIP3P	OPC
OAH									
G1	−5.04 ± 0.01	−6.50 ± 0.23	−6.09 ± 0.28	−7.69 ± 0.01	−8.36 ± 0.37	−4.28 ± 0.38	2.64 ± 0.01	1.86 ± 0.44	−1.81 ± 0.47
G2	−4.25 ± 0.01	−5.42 ± 0.22	−5.16 ± 0.23	−4.39 ± 0.03	−5.71 ± 0.29	−1.83 ± 0.41	0.15 ± 0.03	0.29 ± 0.36	−3.33 ± 0.47
G3	−5.06 ± 0.01	−6.82 ± 0.23	−7.79 ± 0.24	−5.93 ± 0.08	−7.16 ± 0.38	−4.01 ± 0.41	0.87 ± 0.08	0.34 ± 0.44	−3.78 ± 0.48
G4	−9.37 ± 0.00	−12.34 ± 0.23	−11.35 ± 0.29	−14.80 ± 0.01	−15.46 ± 0.38	−9.22 ± 0.36	5.43 ± 0.01	3.12 ± 0.44	−2.13 ± 0.46
G5	−4.50 ± 0.00	**−4.46 ± 0.45** (−4.77 ± 0.24)	−6.42 ± 0.25	−9.90 ± 0.05	−5.57 ± 0.35	−5.60 ± 0.39	5.40 ± 0.05	**1.11 ± 0.57** (0.80 ± 0.42)	−0.82 ± 0.46
G6	−5.33 ± 0.00	−6.46 ± 0.23	−6.41 ± 0.32	−5.67 ± 0.01	−9.50 ± 0.35	−6.82 ± 0.55	0.34 ± 0.01	3.04 ± 0.42	0.41 ± 0.64
OAMe									
G1	−5.24 ± 0.05	−7.61 ± 0.21	−7.88 ± 0.24	−9.96 ± 0.01	−11.73 ± 0.38	−7.79 ± 0.43	4.72 ± 0.05	4.12 ± 0.43	−0.09 ± 0.49
G2	−5.04 ± 0.03	−6.99 ± 0.30	−6.97 ± 0.33	−7.56 ± 0.10	−10.67 ± 0.33	−6.72 ± 0.39	2.52 ± 0.11	3.68 ± 0.45	−0.25 ± 0.51
G3	−5.94 ± 0.12	−7.34 ± 0.22	−8.82 ± 0.24	−6.62 ± 0.18	−9.46 ± 0.42	−6.94 ± 0.32	0.68 ± 0.22	2.12 ± 0.47	−1.88 ± 0.40
G4	−2.38 ± 0.02	**−4.35 ± 0.28** (−1.99 ± 0.23)	**−5.67 ± 0.32** (−0.60 ± 0.27)	-	−13.68 ± 0.34	−5.71 ± 0.42	-	**9.33 ± 0.44** (11.69 ± 0.41)	**0.04 ± 0.53** (5.11 ± 0.50)
G5	−3.90 ± 0.02	−5.30 ± 0.22	−6.64 ± 0.24	-	−6.87 ± 1.03	−7.17 ± 0.45	-	1.57 ± 1.05	0.53 ± 0.51
G6	−4.52 ± 0.02	−6.02 ± 0.21	−7.04 ± 0.25	−9.05 ± 0.13	−11.03 ± 0.37	−7.25 ± 0.44	4.54 ± 0.13	5.01 ± 0.43	0.21 ± 0.51
Error statistics									
R^2		0.83 ± 0.15 (0.90 ± 0.10)	0.68 ± 0.22 (0.77 ± 0.16)		0.51 ± 0.30	0.50 ± 0.21		0.28 ± 0.22 (0.26 ± 0.23)	0.23 ± 0.22 (0.23 ± 0.22)
Slope		1.19 ± 0.22 (1.45 ± 0.17)	0.89 ± 0.25 (1.45 ± 0.47)		0.64 ± 0.34	0.53 ± 0.22		0.37 ± 0.26 (0.35 ± 0.27)	0.27 ± 0.25 (0.27 ± 0.25)
MSE		−1.59 ± 0.22 (−1.42 ± 0.25)	−2.14 ± 0.23 (−1.72 ± 0.37)		−1.31 ± 0.68	2.11 ± 0.62		−0.26 ± 0.61 (−0.29 ± 0.63)	−4.07 ± 0.65 (−4.08 ± 0.64)
MUE		1.62 ± 0.20 (1.49 ± 0.22)	2.14 ± 0.23 (2.01 ± 0.21)		2.18 ± 0.40	2.41 ± 0.50		1.48 ± 0.40 (1.51 ± 0.42)	4.13 ± 0.61 (4.14 ± 0.61)
RMSE		1.74 ± 0.20	2.28 ± 0.21		2.49 ± 0.40	2.84 ± 0.53		1.89 ± 0.48	4.52 ± 0.57

System	G			H			−T S		
	Exp.	TIP3P	OPC	Exp.	TIP3P	OPC	Exp.	TIP3P	OPC
τ		(1.65 ± 0.21) 0.67 ± 0.13 (0.68 ± 0.13)	(2.13 ± 0.19) 0.55 ± 0.18 (0.58 ± 0.18)		0.44 ± 0.27	0.46 ± 0.24		(1.95 ± 0.51) 0.23 ± 0.23 (0.22 ± 0.23)	(4.53 ± 0.57) 0.14 ± 0.26 (0.14 ± 0.26)

Experimental binding free energies (G) and enthalpies (H) are reported as mean ± standard error of the mean (SEM).

The experimental binding data were obtained from Dr. Bruce Gibb [38]. All binding enthalpies and binding affinities of OAH-G6, OAMe-G6 and OAH-G4 were measured by ITC at 298 K in 50 mM sodium phosphate buffer with a pH of 11.5. The binding free energies of the rest systems were measured by NMR at 298 K in 10 mM sodium phosphate with a pH of 11.3 except that OAMe-G4 was measured at 278 K. The same experimental affinities were used for the error analysis in the SAMPL5 overview paper [39].

For binding free energies and entropy terms, values in bold are the corrected affinities of OAH-G5 and OAMe-G4, while values inside the parentheses are based on the submitted predictions. Note that the binding enthalpies are not affected by sampling problems along the pulling pathway because the enthalpy calculations do not depend on the pulling pathway.

The error statistics R^2, slope, MSE, MUE, RMSE and τ are, respectively, the Pearson coefficient of determination, linear regression slope, mean signed error, mean unsigned error and Kendall rank correlation coefficient, respectively. The mean values and uncertainties of the error metrics were obtained through resampling with replacement.